Received: 2 April 2024 | Revised: 22 August 2024 | Accepted: 29 August 2024

DOI: 10.1002/ardp.202400238

ARCH PHARM DPhG
Archiv der Pharmazie

FULL PAPER

iNOS/PGE_2 inhibitors as a novel template for analgesic/anti-inflammatory activity: Design, synthesis, in vitro biological activity and docking studies

Ayca Erdogan[1] | Yagmur Ozhan[2] | Hande Sipahi[2] | Enise Ece Gurdal[3,4] | Wolfgang Sippl[5] | Meric Koksal[1]

[1]Department of Pharmaceutical Chemistry, Faculty of Pharmacy, Yeditepe University, Istanbul, Turkey

[2]Department of Pharmaceutical Toxicology, Faculty of Pharmacy, Yeditepe University, Istanbul, Turkey

[3]Department of Organic Chemistry, Faculty of Chemistry, Martin Luther University Halle-Wittenberg, Halle (Saale), Germany

[4]Department of Nano-Optics, Max Planck Institute for the Science of Light, Erlangen, Germany

[5]Department of Medicinal Chemistry, Institute of Pharmacy, Martin Luther University Halle-Wittenberg, Halle (Saale), Germany

Correspondence
Meric Koksal, Department of Pharmaceutical Chemistry, Faculty of Pharmacy, Yeditepe University, Istanbul 34707, Turkey.
Email: merickoksal@yeditepe.edu.tr

Funding information
Yeditepe University, Grant/Award Number: YAP-AP-SAB-22025

Abstract

Due to the serious gastrointestinal side effects associated with prolonged use of current anti-inflammatory therapies, various strategies such as the regulation of nitric oxide (NO) and prostaglandin E_2 (PGE_2) production have been explored in the field of anti-inflammatory drug development. In this study, a series of disubstituted 1,3,4-oxadiazoles (**3a–f** and **4a–f**) and their cyclized 1,2,4-triazole derivatives (**5a–e** and **6a–e**) were synthesized and tested for their NO, PGE_2, and interleukin-6 (IL-6) releasing inhibition ability. All of the compounds were observed to reduce lipopolysaccharide (LPS)-induced nitrite production in a concentration-dependent manner. Moreover, compounds **3b** (50 µM) and **6d** (1 µM) exhibited 63% and 49% inhibition, respectively, while indomethacin showed 52% at 100 µM. Based on a preliminary NO inhibition assay, 10 of the compounds (**3a**, **3b**, **3e**, **4b**, **4d**, **6a–e**) were selected to be evaluated for in vitro PGE_2, IL-6, and inducible nitric oxide synthase (iNOS) inhibition. Notably, compound **6d** proved to be the most active of the series with the lowest dose (1 µM), in comparison to the other further tested compounds (5–100 µM) and the reference drug indomethacin (100 µM). The inhibitory activity of the compounds was supported by docking simulations into the binding site of the iNOS protein receptor (Protein Data Bank [PDB]ID: 3E7G). The data showing that **4d** reduced iNOS levels the most can be explained by the H-bond with Tyr347 through oxadiazole and π–halogen interactions through the *p*-bromo, in addition to aromatic interactions with protoporphyrin IX.

KEYWORDS
1,2,4-triazolo[3,4-*b*][1,3,4]thiadiazines, 1,3,4-oxadiazoles, anti-inflammatory activity, iNOS/PGE_2 inhibitors, molecular docking

1 | INTRODUCTION

Inflammation is a natural and essential defense mechanism of the body against any harmful stimuli such as pathogens, trauma, or microbial attack. This protective response is characterized by redness, pain, swelling, and heat caused by vascular and cellular changes. The inflammation process can be summarized in stages. First, inflammatory mediators (e.g., prostaglandins, inducible nitric oxide synthase [iNOS], histamine) are released in response to initial injury. This leads to vasodilation and increased vascular permeability. A series of biochemical events and leukocyte migration occurs from blood to the injured tissue. Finally, the proliferation of connective tissue cells leads to a progressive enlargement at the site of initial inflammation.[1,2]

Inflammation can be classified into acute and chronic inflammation based on its duration and severity. While acute inflammation is rapid and short-lived, chronic inflammation develops over time by progression from acute inflammation and triggers various diseases such as atherosclerosis, asthma, cancer, obesity, neurodegenerative disease, and so on.[2–5]

During the inflammatory process, the human immune system employs various immune cells such as monocytes, macrophages, and neutrophils that cooperate with the onset, progression, or resolution of inflammation. Among these, macrophages, as primary proinflammatory cells, create a cellular and molecular inflammatory network when activated, by producing mediators such as nitric oxide (NO), prostaglandin E_2 (PGE_2), tumor necrosis factor α (TNF-α), and interleukins (ILs).[6,7] Moreover, lipopolysaccharide (LPS) is one of the key components that can promote the activation of macrophages and stimulate receptors in these cells leading to the release of transcription factors and inflammatory mediators.[8,9] Therefore, controlling the production of NO and PGE_2 in LPS-stimulated macrophages is considered an excellent model for the screening and evaluation of potent anti-inflammatory agents[7,8,10] (Figure 1).

The role of inflammation in the development of numerous diseases, and the presence of serious gastrointestinal side effects associated with the long-term use of current anti-inflammatory drugs, still highlights the necessity for a safe and effective inflammation treatment. Thus, to accomplish this present major challenge, different strategies have been reported, including the design of molecules, that show their anti-inflammatory activity through another mechanism than direct COX inhibition, or replacing the carboxylic acid functional group in classical nonsteroidal anti-inflammatory drugs (NSAIDs) with less acidic bioisosteres.[11–13] One promising approach involves developing iNOS inhibitor hybrids of marketed NSAIDs, which show anti-inflammatory effects by suppressing the overexpression of NO, PGE_2, and IL-6.[11,14–16] In recent years, compounds containing 1,3,4-oxadiazole and 1,2,4-triazole nuclei have been documented as potent anti-inflammatory agents with improved pharmacokinetic and physicochemical profiles.[17,18] Considering the published studies, pharmacophore groups of anti-inflammatory agents with 1,3,4-oxadiazole and 1,2,4-triazole nuclei were determined. As a result of docking

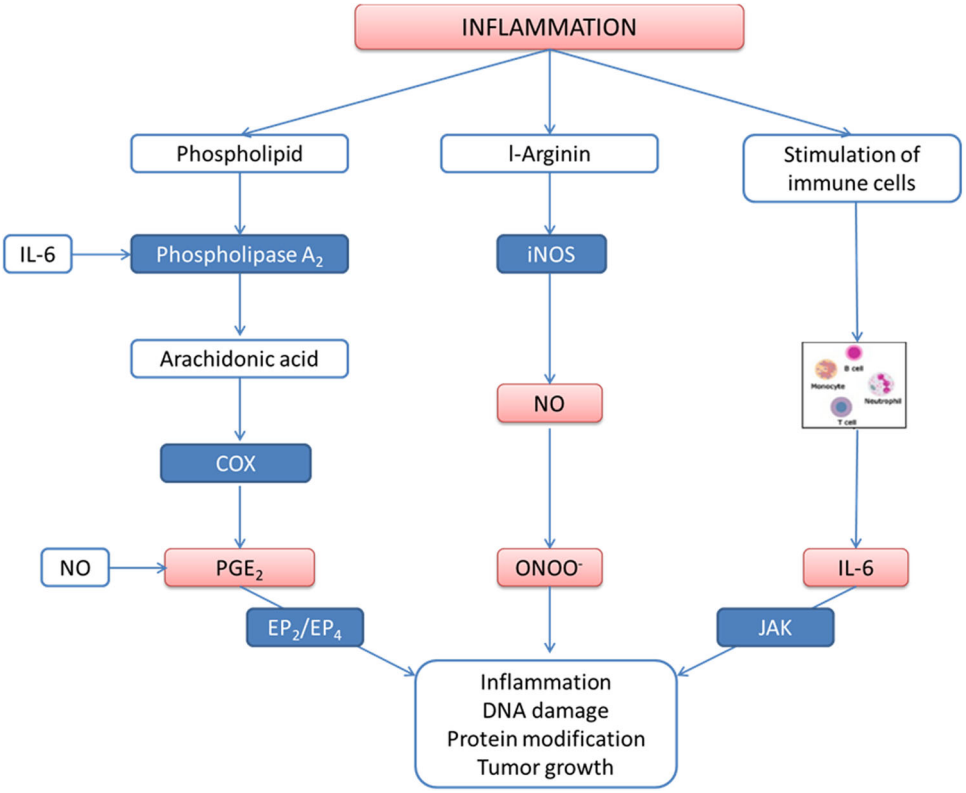

FIGURE 1 Circuit representation of inflammation. Interleukin-6 (IL-6), iNOS, and prostaglandin E_2 (PGE_2) are the basic nodes of the circuit that represent the basic features of inflammation. In this circuit, the arrows represent activation. PGE_2 leads to prolonged inflammation inducing EP2/EP4. iNOS produces ONOO (peroxynitrite)- radicals and IL-6 stimulates JAK contributing to the inflammation process. EP2/EP4, prostaglandin E2 receptor subtypes 2 (EP2) /prostaglandin E2 receptor subtypes 4 (EP4); JAK, Janus kinase.

studies of identified pharmacophore groups on iNOS, new 1,3,4-oxadiazoles (**3a–f**, **4a–f**) and their cyclized 1,2,4-triazolo[3,4-*b*][1,3,4] thiadiazine derivatives (**5a–e**, **6a–e**) were designed as anti-inflammatory agents targeting iNOS, PGE_2, and IL-6.

This study reports various 1,3,4-oxadiazole and their fused bicyclic triazolothiadiazine analogs as multitarget anti-inflammatory agents (Figure 2). The activities of the target compounds were primarily evaluated by measuring the inhibition of NO production in LPS-activated murine macrophage RAW264.7 which is a fast, cheap, and reliable test for identifying the potentially active derivatives. Further, the compounds with IC_{50} values < 100 μM were selected to be evaluated for in vitro PGE_2, IL-6, and iNOS inhibitory activity. Specifically, molecular docking studies were performed to identify the interactions of the potent derivatives as PGE_2/iNOS dual inhibitors with the targeted iNOS enzyme.

2 | RESULTS AND DISCUSSION

2.1 | Chemistry

New 1,3,4-oxadiazole (**3a–f**, **4a–f**) and 1,2,4-triazolo[3,4-*b*][1,3,4]thiadiazine derivatives (**5a–e**, **6a–e**) were synthesized as outlined in Scheme 1. The starting materials **1a**, **1b** were prepared according to the previously reported procedure.[19] The aroyl hydrazine **1a**, **1b** were reacted with carbon disulfide and potassium hydroxide, and the resulting mixture was refluxed to obtain two different 5-aryl-1,3,4-oxadiazole-2-thiones **2a**, **2b**. *S*-Alkylation of the rings was performed with appropriate phenacyl bromides in a basic medium. In the final step of the synthetic pathway, the *S*-alkyl-1,3,4-oxadiazole derivatives **3a–f**, **4a–f** were cyclized with hydrazine hydrate to yield corresponding 1,2,4-triazolo[3,4-*b*]-1,3,4-thiadiazines **5a–e**, **6a–e** (Scheme 1). The structural characterization of novel oxadiazole and triazolothiadiazine derivatives was carried out using their FT- Infrared (IR), ^{1}H-NMR, ^{13}C-NMR, and elemental analysis. FT-IR, ^{1}H-NMR, and ^{13}C-NMR results of all the synthesized compounds are compatible with the depicted structures. However, because of the solubility problems, ^{13}C-NMR of some compounds could not be analyzed. Additionally, ultra performance liquid chromatography (UPLC) profiles of synthesized compounds were presented for purity profiling.

The identification of the *S*-alkyl oxadiazole analogs **3a–f**, **4a–f** with IR spectrum was evaluated based on the disappearance of the C=S bond. Similarly, the absence of characteristic strong C=O absorption bands in approximately 1680 cm^{-1} was substantiated by the ring closure reaction of triazolothiadiazine derivatives **5a–e**, **6a–e**. In the ^{1}H-NMR, the analysis of the aliphatic region with the appearance of a methylene singlet at δ 5.11–5.22 and δ 4.41–4.44 ppm, confirmed the formation of all expected 1,3,4-oxadizole and 1,2,4-triazolo[3,4-*b*]1,3,4-thiadiazines, respectively as well as aromatic protons at their expected chemical shifts. Based on the ^{13}C-NMR results, the signals at δ 163.58–165.74 ppm and δ 142.03–152.76 ppm were also detected as carbons on 1,3,4-oxadizole and 1,2,4-triazolo[3,4-*b*]-1,3,4-thiadiazine moiety.

2.2 | Pharmacology/biology

2.2.1 | Cell viability

To determine safe and nontoxic concentrations of each compound, cytotoxicity testing was carried out before in vitro anti-inflammatory activity screening. Safe doses of compounds were determined via cell viabilities that were above 70% in comparison to the lipopolysaccharide (+) (LPS (+)) (Figure 3).

2.2.2 | NO inhibition assay

The in vitro anti-inflammatory activities of the molecules were evaluated by observing the decrease in nitrite production levels using the Griess reagent. The molecules were tested for their inhibitory activity against LPS-induced nitrite production in RAW264.7 cells. Indomethacin and L-NAME (Nω-nitro-L-arginine methyl ester hydrochloride), known for their anti-inflammatory properties, were used as reference molecules in this study.

The effects of compounds on nitrite production in RAW264.7 cells are shown in Figure 4. Compounds **6d** (0.1 μM) and **6e** (50 μM) presented a higher effect on nitrite production. Using these data, NO inhibition and IC_{50} values of the compounds are calculated and summarized in Table 1. All molecules were observed to reduce LPS-induced nitrite production in a concentration-dependent manner. NO inhibition results point out that the cyclization of 1,3,4-oxadiazole compounds gives more active derivatives (**6a–e**). However, the compounds **3a**, **3b**, **3e**, **4b**, and **4d** also exhibited excellent nitrite-suppressor activity, compared with indomethacin. The activity of some derivatives (**5b–e**) could not be analyzed due to solubility problems. All 3,5-dimethyl substituted derivatives of 1,2,4-triazolo[3,4-*b*][1,3,4] thiadiazine (**6a–e**) showed potent NO inhibition activity with

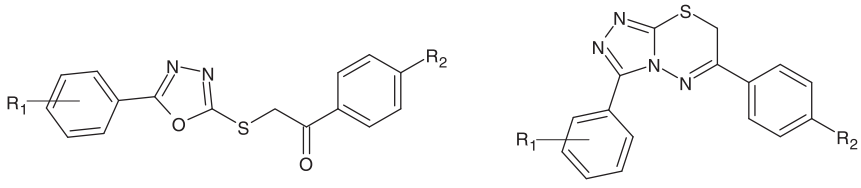

FIGURE 2 Structures of the target compounds.

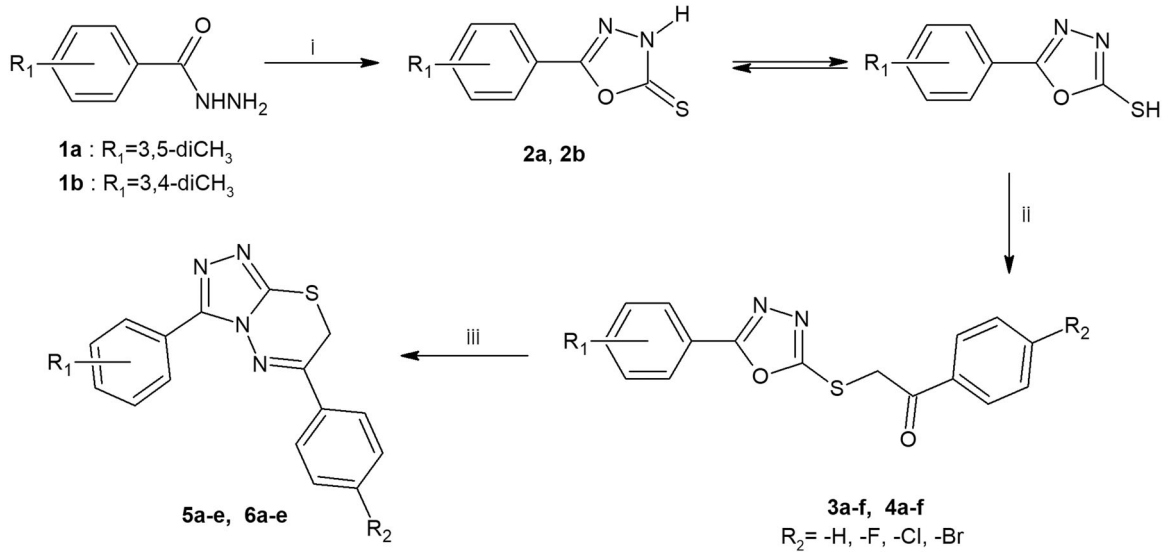

SCHEME 1 Synthetic routes to 1,3,4-oxadiazole and 1,2,4-triazolo[3,4-*b*][1,3,4]-thiadiazine derivatives. Reagents and conditions: (i) KOH, CS_2, reflux, 8 h; (ii) $ArCOCH_2Br$, C_2H_5ONa, 25°C, 9 h; and (iii) $H_2NNH_2.H_2O$, CH_3COOH, reflux, 4 h.

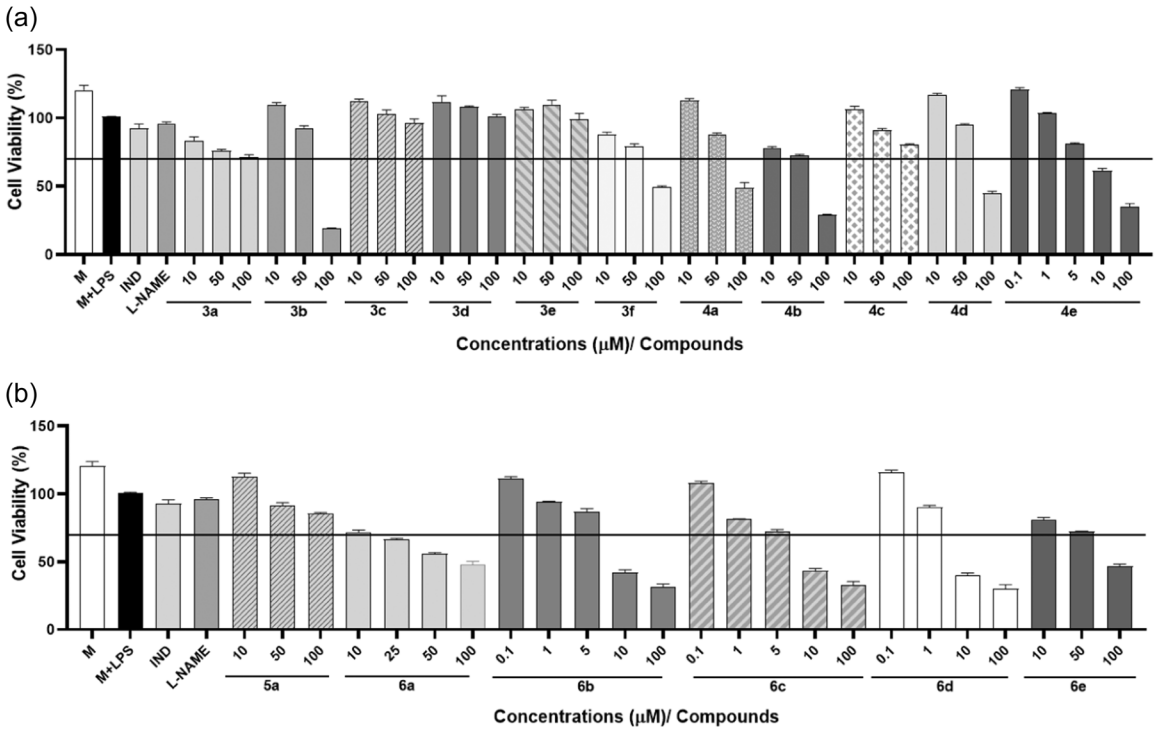

FIGURE 3 Effects of compounds on the viability of RAW264.7 macrophage cells. (a) Oxadiazole derivatives (**3a–f**, **4a–f**), (b) triazolothiadiazine derivatives (**5a–e**, **6a–e**). Cell viability of the compounds was compared with the untreated control group (medium group) and groups with cell viability below 70% were considered cytotoxic. IND, indomethacin (100 μM); LPS, lipopolysaccharides from *Escherichia coli*; L-NAME, Nω-nitro-L-arginine methyl ester hydrochloride (100 μM).

0.21–26.60 μM IC_{50} values. Compound **6b** with fluoro, **6c** with chloro, and **6d** with bromo atoms are the most active derivatives among the two series, having respectively 4.78, 3.97, and 0.21 μM IC_{50}. Also, these results reveal that halogen fragments have a significant role in NO inhibition in these derivatives. When looking at nitrite inhibition, it was observed that **6d** possessed the most active anti-inflammatory effect. Compound **6d** was selected to be an interesting compound, showing almost the same effect with a test dose of 1 μM as indomethacin at 100 μM.

In conclusion, compounds **3a**, **3b**, **3e**, **4b**, **4d**, and **6a–e**, whose NO inhibition activities were below <100 μM IC_{50}, were selected to evaluate their effects on inflammation markers. The experimentally

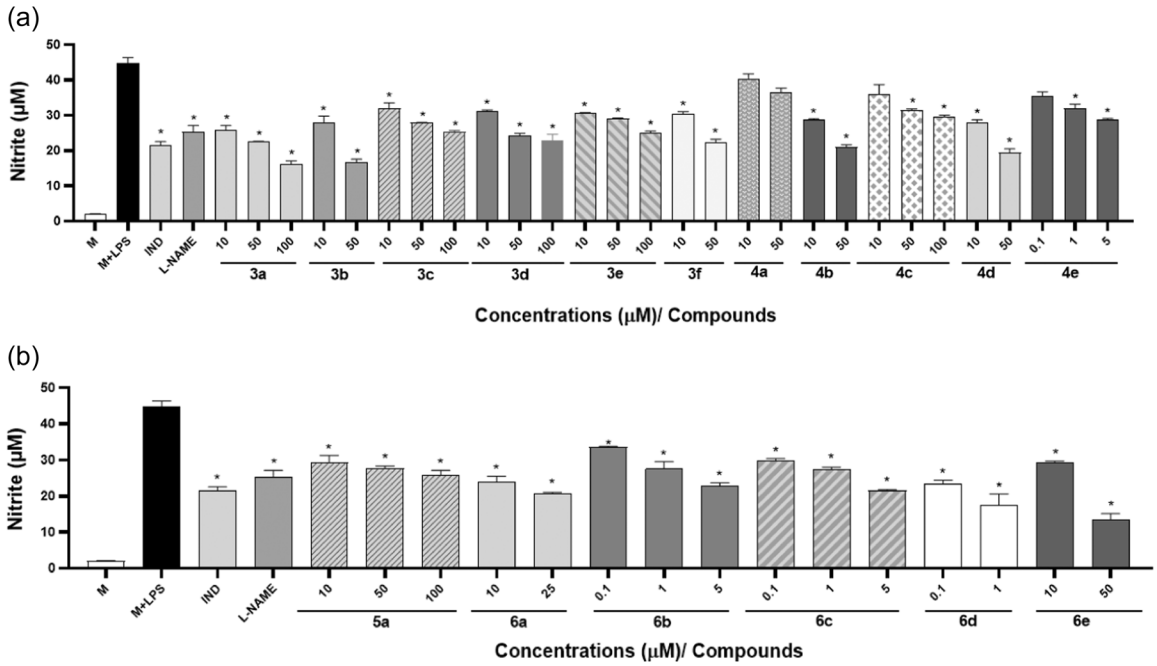

FIGURE 4 Effects of compounds on nitrite production in RAW264.7 cells stimulated with 1 μg/mL LPS. (a) Oxadiazole derivatives (**3a–f**, **4a–f**), (b) triazolothiadiazine derivatives (**5a–e**, **6a–e**). INDI indomethacin (100 μM); LPS, lipopolysaccharides from *Escherichia coli*; L-NAME, Nω-nitro-L-arginine methyl ester hydrochloride (100 μM). Statistically significant differences are indicated for each compound versus LPS (*$p < 0.001$).

tested concentrations of these compounds showing the highest anti-inflammatory activity were used in these studies.

2.2.3 | PGE_2 inhibition assay

PGE_2, one of the products of the arachidonic acid pathway, is considered as an important parameter in the evaluation of analgesic activity. PGE_2 levels are detected in LPS (1 μg/mL)-stimulated RAW264.7 murine macrophage cells by using an enzyme-linked immunosorbent assay (ELISA) kit method and are presented in Table 2. As a result, while the PGE_2 level in the control group was 17.93 ± 1.02 pg/mL; it was observed that the PGE_2 level in the 1 μg/mL LPS applied group was 249.50 ± 2.48 pg/mL. While all compounds significantly reduced the LPS-induced PGE_2 level, the derivatives bearing 5-(3,5-dimethyl)-1,3,4-oxadiazole moiety (**3a–f**) exhibited stronger inhibitory activity than the other derivatives on PGE_2. Indomethacin, used as a positive control, reduced the PGE_2 level by 88% compared with the LPS group. Among the compounds, it was seen in the table that compound **3b** (90%) had the highest analgesic activity at the doses studied.

2.2.4 | IL-6 releasing inhibition assay

In response to LPS stimulation, macrophages could also release proinflammatory cytokines, such as IL-6, which is known as a multifunctional cytokine, and it has proinflammatory and immuno-regulatory functions. L-NAME and indomethacin were used as positive controls to compare the potency of compounds on IL-6. As shown in Table 2, the IL-6 level in the control group was 133.05 ± 1.15 pg/mL, while it was found to be 2080.69 ± 94.44 pg/mL in the presence of LPS. Compared with the LPS group, indomethacin, as a standard anti-inflammatory drug, reduced IL-6 levels by 72%. It was also observed that all compounds significantly reduced LPS-induced IL-6 levels. Considering the data, it was seen that **3b** (50 μM) was the one that reduced the IL-6 level the most (72%) among the compounds. It was concluded that the effects of indomethacin and compound **3b** on IL-6 inhibition were similar. However, compound **3b** showed this effect at half the dose of indomethacin. Additionally, low-dose administration of compounds **4d** (50 μM), **6b** (5 μM), and **6d** (1 μM) in the series was also observed to significantly reduce LPS-increased IL-6 levels with approximately 69% for three compounds.

2.2.5 | iNOS inhibition assay

While the iNOS level of the control group was 66.85 ± 0.40 pg/mL, in the LPS group, the iNOS level was calculated as 3306.68 ± 82.58 pg/mL. All compounds were observed to significantly reduce the iNOS level (Table 2). It was found that indomethacin reduced the iNOS level by 90% compared with the LPS group. It was emphasized that the derivatives **3b**, **4d**, and **6d**, which were the most active ones on PGE_2 and IL-6 inhibition, also showed the highest inhibition on iNOS. Based on the results, it was observed that compounds **3b**, **4b**, **4d**, **6a**, **6d**, and **6e**

TABLE 1 NO suppression activities of the synthesized compounds.

Compounds	R_1	R_2	Dose (μM)	NO inhibition (%) ± S.D.	NO inhibition IC_{50} (μM) ± S.D.
Control				-	-
Indomethacin			100	51.83 ± 4.00	-
L-NAME			100	43.42 ± 1.95	-
			10	42.13 ± 2.05	
3a	3,5-Dimethyl	–H	50	50.13 ± 2.02	46.83 ± 3.67
			100	64.07 ± 1.42	
			10	38.78 ± 3.18	
3b	3,5-Dimethyl	–F	50	62.90 ± 2.52	30.01 ± 1.98
			100	-	
			10	26.90 ± 3.66	
3c	3,5-Dimethyl	–Cl	50	38.26 ± 1.86	>100
			100	43.84 ± 1.93	
3d	3,5-Dimethyl	–Br	10	30.14 ± 2.67	>100
			50	46.47 ± 0.41	
3e	3,5-Dimethyl	$-CH_3$	10	32.45 ± 2.21	47.28 ± 1.93
			50	50.61 ± 1.51	
			100	-	
3f	3,5-Dimethyl	$-NO_2$	10	31.87 ± 2.65	>100
			50	35.99 ± 2.80	
			100	44.44 ± 1.96	
4a	3,4-Dimethyl	–H	10	9.85 ± 5.20	>100
			50	19.11 ± 1.55	
			100	-	
4b	3,4-Dimethyl	–F	10	35.82 ± 1.74	39.08 ± 4.06
			50	53.57 ± 2.86	
			100	-	
4c	3,4-Dimethyl	–Cl	10	25.90 ± 9.72	>100
			50	30.48 ± 1.55	
			100	34.79 ± 1.11	
4d	3,4-Dimethyl	–Br	10	37.61 ± 2.62	29.49 ± 8.57
			50	57.01 ± 3.19	
			100	-	
4e	3,4-Dimethyl	$-CH_3$	0.1	21.86 ± 0.39	>100
			1	29.28 ± 0.15	
			5	36.63 ± 1.33	
			10	-	
			100	-	
5a	3,5-Dimethyl	–H	10	34.37 ± 5.28	>100
			50	38.69 ± 0.68	
			100	42.91 ± 4.88	

TABLE 1 (Continued)

Compounds	R_1	R_2	Dose (μM)	NO inhibition (%) ± S.D.	NO inhibition IC_{50} (μM) ± S.D.
6a	3,4-Dimethyl	–H	10	46.51 ± 3.89	17.00 ± 0.33
			25	54.25 ± 0.71	
			50	-	
			100	-	
6b	3,4-Dimethyl	–F	0.1	26.30 ± 2.38	4.78 ± 0.06
			1	39.15 ± 2.23	
			5	50.26 ± 0.28	
			10	-	
			100	-	
6c	3,4-Dimethyl	–Cl	0.1	34.45 ± 0.45	3.97 ± 0.41
			1	39.46 ± 3.55	
			5	52.38 ± 2.23	
			10	-	
			100	-	
6d	3,4-Dimethyl	–Br	0.1	48.49 ± 0.75	0.21 ± 0.02
			1	61.60 ± 7.84	
			10	-	
			100	-	
6e	3,4-Dimethyl	$-CH_3$	10	34.61 ± 2.28	26.60 ± 1.08
			50	70.07 ± 2.43	
			100	-	

Abbreviations: L-NAME, Nω-nitro-L-arginine methyl ester hydrochloride; NO, nitric oxide.

TABLE 2 Effects of compounds on PGE_2, IL-6, and iNOS levels in RAW264.7 cells stimulated with 1 μg/mL LPS.

Groups	Dose (μM)	PGE_2 (pg/mL)	IL-6 (pg/mL)	iNOS (pg/mL)
Control		17.93 ± 1.02	133.05 ± 1.15	66.85 ± 0.40
Control+LPS		**249.50 ± 2.48**	**2080.69 ± 94.44**	**3306.68 ± 82.58**
Indomethacin	100	**29.25 ± 1.78***	**588.36 ± 7.33***	**343.91 ± 13.60***
3a	100	35.40 ± 8.37*	1671.21 ± 29.51*	2446.82 ± 135.01*
3b	50	**24.73 ± 1.26***	**577.55 ± 3.03***	**374.33 ± 20.01***
3e	50	39.43 ± 1.51*	1218.72 ± 4.17*	2381.90 ± 47.25*
4b	50	54.77 ± 4.58*	1482.98 ± 10.63*	708.86 ± 7.34*
4d	50	80.99 ± 9.52*	646.86 ± 9.00*	**201.01 ± 8.15***
6a	25	137.18 ± 27.66*	1522.54 ± 3.10*	712.83 ± 15.37*
6b	5	81.56 ± 6.02*	827.28 ± 6.82*	1327.43 ± 50.37*
6c	5	72.55 ± 3.91*	654.11 ± 10.43*	1758.00 ± 37.91*
6d	1	**30.60 ± 2.73***	**643.34 ± 8.54***	568.08 ± 6.37*
6e	50	52.26 ± 3.06*	1322.41 ± 2.69*	465.99 ± 11.25*

Note: Statistically significant differences are indicated for each compound versus LPS (*$p < 0.001$).

Abbreviations: IND, indomethacin (100 μM); IL-6, interleukin-6; iNOS, inducible nitric oxide synthase; LPS, lipopolysaccharides from *Escherichia coli*; PGE_2, prostaglandin E_2.

significantly reduced the iNOS level. Among these compounds, the one that reduced the iNOS level the most was **4d** with a rate of 94%.

2.3 | Molecular docking

Docking studies were carried out to predict the interactions of the compounds within the binding site of iNOS (Protein Data Bank [PDB] ID: 3E7G [20]). The co-crystallized AR-C95791 ligand (redocking score (ds): −5.60, RMSD: 0.595 Å) is involved in π–π and π–cation interactions with protoporphyrin IX and makes H-bonds with Tyr347 and Glu377 residues. Compounds **3a–f** and **4a–f** were docked in a region similar to the co-crystallized inhibitor and showed H-bonds between the carbonyl groups and Tyr373 as well as between the oxadiazole N atom and Tyr347, respectively (Figure 5). Since compounds **5a–e** and **6a–e** cannot make such an H-bond, they prefer hydrophobic and aromatic π–π/π–halogen interactions, especially with Phe369 and Tyr491, and are positioned toward the tunnel entrance of the protein (Figure 6).

When the interactions of the compounds with protoporphyrin IX are examined in detail, it is seen that the compounds **3a**, **3b**, **3e**, **4b**, and **4d** have strong π–π and π–cation interactions as a result of parallel positioning, similar to the co-crystallized inhibitor (Figures 7 and 8). For the compounds, **6b**, **6c**, and **6d**, only π–π interactions seem possible as a result of interference perpendicular to protoporphyrin IX. The previously mentioned hydrophobic and aromatic interactions play a fundamental role in keeping this interaction stable (Figure 9).

Finally, following the in vitro inhibitory test results of compound **4d**, docking studies revealed that the position of compound **4d** is similar to the co-crystallized ligand in the binding site of iNOS making appropriate aromatic interactions with protoporphyrin IX, H-bonds with Tyr347 via oxadiazole and π–halogen interactions via *p*-bromo group (Figure 10). Docking scores for all molecules are shown in Table 3.

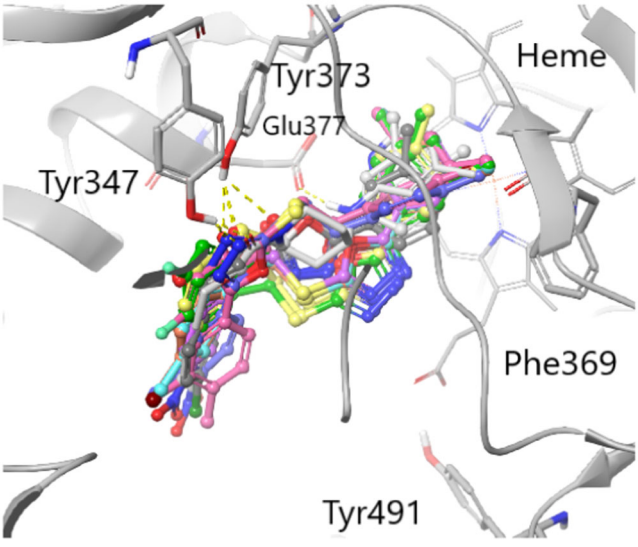

FIGURE 5 Binding pose of compound groups encoded as **3** and **4** in iNOS enzyme (Protein Data Bank [PDB] ID: 3e7g, H-bonds are shown as yellow dashed lines). iNOS, inducible nitric oxide synthase.

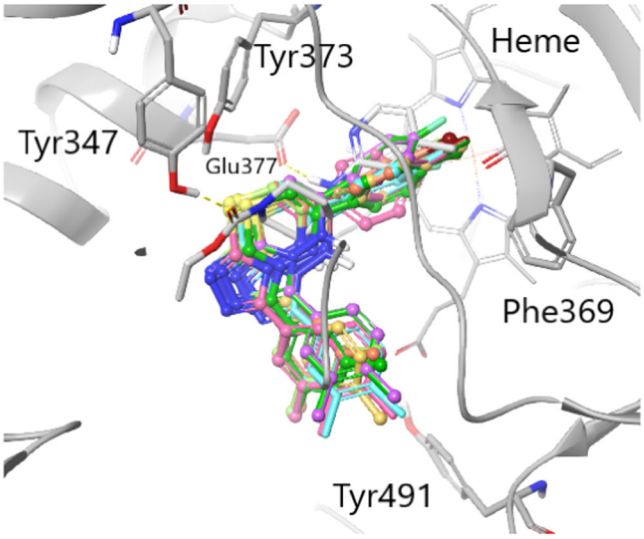

FIGURE 6 Binding pose of compound groups encoded as **5** and **6** in iNOS enzyme (Protein Data Bank [PDB] ID: 3e7g, H-bonds are shown as yellow dashed lines). iNOS, inducible nitric oxide synthase.

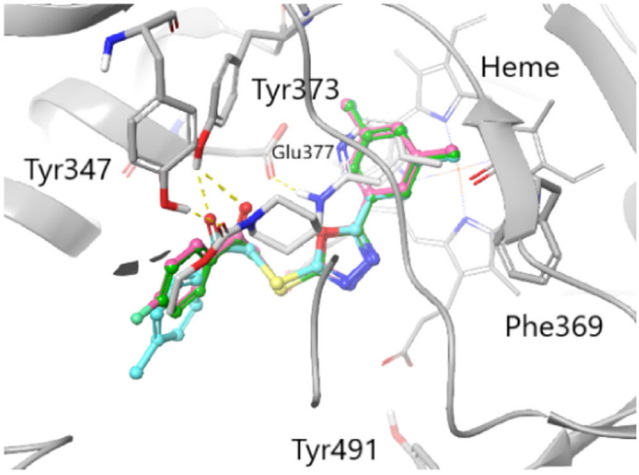

FIGURE 7 Binding poses of the co-crystallized ligand (gray) with compounds **3a** (green), **3b** (pink), and **3e** (cyan) in iNOS enzyme (Protein Data Bank [PDB] ID: 3e7g, H-bonds are shown as yellow dashed lines). iNOS, inducible nitric oxide synthase.

3 | CONCLUSION

In this study, two sets of compounds from 1,3,4-oxadiazole and 1,2,4-triazolo[3,4-*b*][1,3,4]thiadiazine were designed as dual iNOS/PGE_2 inhibitor anti-inflammatory agents. After that, docking studies were performed to investigate the binding pattern of the designed molecules with the iNOS enzyme. These studies have proven that the presence of three moieties including oxadiazole,

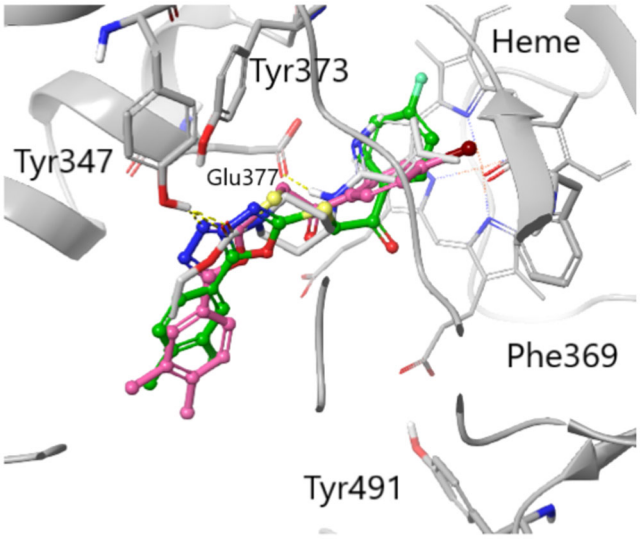

FIGURE 8 Binding poses of the co-crystallized ligand (gray) with compounds **4b** (green) and **4d** (pink) in iNOS enzyme (Protein Data Bank [PDB] ID: 3e7g, H-bonds are shown as yellow dashed lines). iNOS, inducible nitric oxide synthase.

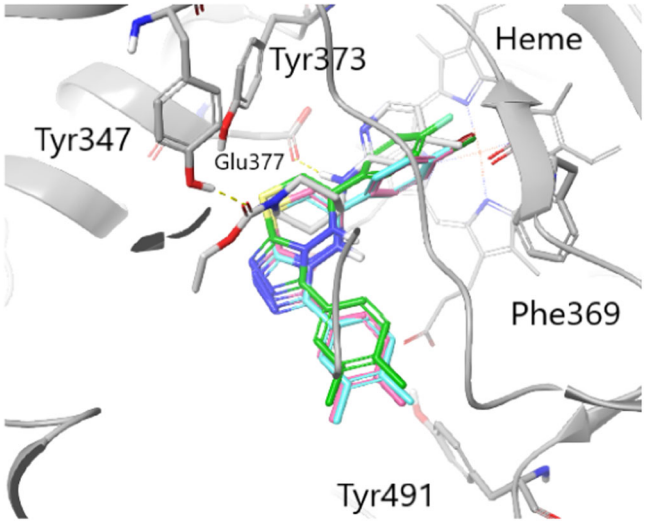

FIGURE 9 Binding poses of the co-crystallized ligand (gray) with compounds **6b** (green), **6c** (pink), and **6d** (cyan) in iNOS enzyme (Protein Data Bank [PDB] ID: 3e7g, H-bonds are shown as yellow dashed lines). iNOS, inducible nitric oxide synthase.

carbonyl, and aromatic structures on compounds **3a–e**, **4a–e** is important: oxadiazole for H bond with Tyr347, carbonyl group for H bond with Tyr373, and aromatic groups for π–π interaction. It has been observed that compounds with a 1,2,4-triazole nucleus (**5a–e**, **6a–e**) are positioned at the tunnel entrance of the protein by aromatic π–π/ /π–halogen interactions. After the synthesis of 22 molecules including 10 Chemical abstracts service (CAS) registered 1,3,4-oxadiazole derivatives, all compounds were characterized with spectral analysis, and their purities were checked by elemental analysis and UPLC since neither physical nor any structural data were reported for registered compounds. All the confirmed compounds

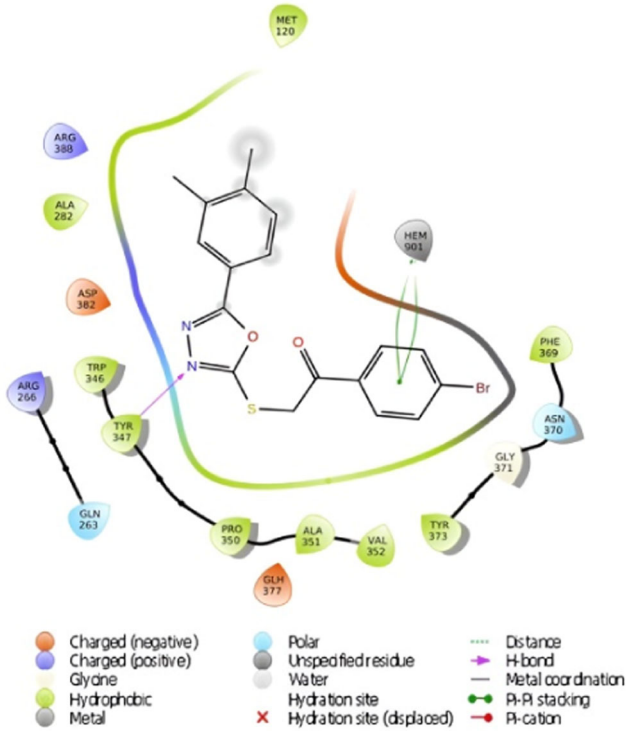

FIGURE 10 Two-dimensional (2D) representation of the interactions of compound **4d** with the iNOS enzyme (Protein Data Bank [PDB] ID: 3e7g). iNOS, inducible nitric oxide synthase.

TABLE 3 Docking scores of the compounds.

Compound	Docking score	Compound	Docking score
3a	−5.57	**5a**	−4.24
3b	−5.35	**5b**	−3.80
3c	−5.05	**5c**	−4.33
3d	−5.26	**5d**	−4.06
3e	−5.40	**5e**	−4.32
3f	−4.50	**6a**	−4.50
4a	−5.02	**6b**	−4.43
4b	−4.83	**6c**	−4.78
4c	−4.76	**6d**	−4.45
4d	−4.60	**6e**	−4.85
4e	−4.73	AR-C95791	−5.60
4f	−4.46		

were tested for their anti-inflammatory activity using in vitro test methods. Even if NO inhibition data show that compounds **3b** and **6d** exhibited significant inhibitions on NO productions in LPS-induced RAW264.7 cells with 63% and 49% inhibition values respectively at 50 and 1 μM doses while indomethacin showed 52% inhibition activity at 100 μM. Based on the NO inhibition result, the effect of

selected compounds over inflammation mediators was investigated at noncytotoxic doses. All the tested compounds exhibited inhibition on all markers in different ranges, however, compounds **3b** and **6d** at low doses had higher inhibitory activity on three inflammation markers than indomethacin against PGE_2, IL-6, and iNOS. Compound **3b** exhibited almost a similar activity profile with the reference drug at 50 µM, which is half the concentration of indomethacin. While indomethacin showed 88% PGE_2, 72% IL-6, and 90% iNOS inhibition, compound **6d** achieved 88% PGE_2, 69% IL-6, and 83% iNOS inhibition at 1 µM tested dose. In the enzymatic level, compound **4d** was also determined to be the compound that reduced the iNOS enzyme level the most (94%). This activity of the compound can be explained by the H-bond with Tyr347 through oxadiazole and the π–halogen interactions through the *p*-bromo group, in addition to the aromatic interactions also shown by other derivatives in docking studies. All activity results realized that the cyclization of 1,3,4-oxadiazoles (**3a–e**, **4a–e**) gives more active derivatives. According to the docking results, unlike the other compounds in the series, compounds **5a–e** and **6a–e** prefer hydrophobic and aromatic π–π/ / π–halogen interactions, which may be the reason for their stronger activities. Due to the solubility problem, the missing data in the activities of compounds **5b–e** made it difficult to establish the structure–activity relationship. Based on the activity data of compounds **6a–e**, the presence of halogen (F, Cl, Br) reinforces the anti-inflammatory and analgesic activity. Among the compounds containing halogen, the bromine derivative **6d** (1 µM), which has less electronegativity, was found to be 100 times more active than the reference substance. This confirms that the compounds **3b**, **4d**, and **6d** are promising compounds exhibiting strong anti-inflammatory and analgesic properties through multiple therapeutic targets that lead to the maintenance and progression of inflammation. Thus, compounds **3b**, **4d**, and **6d** were chosen as the hit compounds to elucidate further their anti-inflammatory activities and toxicological profiles with in vivo studies due to their potent effects at low concentrations.

4 | EXPERIMENTAL

4.1 | Chemistry

4.1.1 | General

All reagents were purchased from commercial sources and were used without further purification. The reactions were monitored by thin layer chromatography on Merck pre-coated silica gel GF254 plates using UV light (254/365 nm) for visualization. Melting points were determined by using a Mettler Toledo FP62 capillary melting point apparatus (Mettler-Toledo) and were uncorrected. Synthesized compounds were characterized by using FT-IR, ^{1}H-, and ^{13}C-NMR spectroscopies, elementary, and UPLC analysis. Infrared spectra were recorded on a Perkin-Elmer Spectrum One series FT-IR apparatus (version 5.0.1) (Perkin-Elmer) using KBr pellets, and the frequencies were expressed in cm^{-1}. The ^{1}H- and ^{13}C-NMR spectra (see the Supporting Information) were recorded with a Varian Mercury-400 FT-NMR spectrometer (Varian), using tetramethylsilane as the internal reference, with dimethylsulfoxide (DMSO) or pyridine (only for dissolvable compounds) as a solvent, respectively. The chemical shifts were reported in parts per million (ppm), and coupling constants (J) were given in Hertz (Hz). Elemental analyses were performed on a LECO 932 CHNS instrument (Leco-932). UPLC analyses were performed on Nexera UPLC Series (Schimadzu).

The InChI codes of the investigated compounds, together with some biological activity data and the structural elucidation data, are provided as Supporting Information.

4.1.2 | UPLC method to determine the purity

UPLC analysis was performed using the UPLC system (Schimadzu), consisting of a quarternary pump, an autosampler, a thermostatted column compartment, and a photodiode array (PDA) detector. The UPLC system was operated by LabSoluntions software (5.111). Analysis was carried out on a ZORBAX Eclipse XDB-C8 Column (4.6 × 150 mm I.D., 5-micron particle size, Agilent. The column temperature was set to 25°C. Mobile phase for all compounds **3a–f** and **4a–f** was a mixture of distilled water (20%) and acetonitrile (80%). Mobile phase for **5a–e** and **6a–e** was distilled water (30%) and acetonitrile (70%). The mobile phases were degassed and filtered through a 0.2 µM filter before analyses. The isocratic elutions with flow rate were applied as 1 mL/min. The injection volume was 5 µM.

4.1.3 | General procedure for the synthesis of 2a,b

To a solution of corresponding acyl hydrazide **1a**, **1b** (3.13 mmol) and carbon disulfide (6.27 mmol) in absolute ethanol (15 mL), potassium hydroxide was added and then the mixture was refluxed for 8 h. Upon completion, the solvent was evaporated under reduced pressure, and the residue was dissolved in water. The aqueous solution was acidified to pH=2 using hydrochloric acid (2 mol/L) and extracted with ethyl acetate (2 × 20 mL). The organic layers were washed with water and collected together to be dried with anhydrous sodium sulfate. Filtration and concentration in vacuo gave appropriate 1,3,4-oxadiazole-5-thiones **2a**, **2b** which were crystallized from ethanol.[20,21]

4.1.4 | General procedure for the synthesis of 3a–f and 4a–f

Dimethylphenyl-1,3,4-oxadiazole-2-thione **2a**, **2b** (10 mmol) was dissolved in sodium alcoholate (10 mmol/25 mL), and the solution was refluxed for 4 h. The appropriate phenacyl bromide (10 mmol) was then added and refluxed for a further 9 h. After completion of the reaction (monitored with TLC), the mixture was poured into ice water, the precipitate was collected by filtration, washed with water, dried, and recrystallized from acetone to obtain **3a–f** and **4a–f**.[19]

5-(3,5-Dimethylphenyl)-2-(benzoylmethyl)thio-1,3,4-oxadiazole (**3a**) (CAS Registry number: 1004367-92-3): Yield: 80%; mp: 149°C; Purity (UPLC): t_R = 5.24 min, purity 99.9%. FT-IR υ_{max} (KBr, cm^{-1}): 2922 (CH aromatic), 1681 (C=O), 1558 (C=C aromatic), 1474 (C=N). ^{1}H-NMR (400 Hz, DMSO-d_6, ppm): δ = 8.07 (d, 2H, J = 8 *Hz* benzoyl H_{2+6}), 7.74 (t, 1H, J = 6 *Hz* benzoyl H_4), 7.60 (d, 2H, J = 8 *Hz* benzoyl H_{3+5}), 7.54 (s, 2H, dimethylphenyl H_{2+6}), 7.24 (s, 1H, dimethylphenyl H_4), 5.17 (s, 2H, $-CH_2-$), 2.33 (s, 6H, $-CH_3$). ^{13}C-NMR (400 Hz, DMSO-d_6, ppm): δ = 193.24 (C=O), 165.74 (oxadiazole C_5), 163.58 (oxadiazole C_2), 139.24, 135.58, 134.53, 133.91, 129.39, 128.99, 124.39, 123.23, 40.92 ($-CH_2-$), 21.16 ($-CH_3$). Elemental Analysis Calcd. (%) for $C_{18}H_{16}N_2O_2S$ (324.40): C, 66.64; H, 4.97; N, 8.64; S, 9.88. Found: C, 66.55; H, 4.74; N, 8.62; S, 9.80.

5-(3,5-Dimethylphenyl)-2-[(4-fluorobenzoyl)methyl]thio-1,3,4-oxadiazole (**3b**) (CAS Registry number: 460043-51-0): Yield: 69%; mp: 153°C; Purity (UPLC): t_R = 5.49 min, purity 100%. FT-IR υ_{max} (KBr, cm^{-1}): 2954 (CH aromatic), 1684 (C=O), 1594 (C=C aromatic), 1473 (C=N). ^{1}H-NMR (400 Hz, DMSO-d_6, ppm): δ = 8.16 (d, 2H, J = 7.1 *Hz* benzoyl H_{3+5}), 7.40 (d, 2H, J = 7.1 *Hz* benzoyl H_{2+6}), 7.52 (s, 2H, dimethylphenyl H_{2+6}), 7.24 (s, 1H, dimethylphenyl H_4), 5.14 (s, 2H, $-CH_2-$), 2.32 (s, 6H, $-CH_3$). Elemental Analysis Calcd. (%) for $C_{18}H_{15}FN_2O_2S$ (342.39): C, 63.14; H, 4.42; N, 8.18; S, 9.37. Found: C, 63.15; H, 4.29; N, 8.21; S, 9.32.

5-(3,5-Dimethylphenyl)-2-[(4-chlorobenzoyl)methyl]thio-1,3,4-oxadiazole (**3c**) (CAS Registry number: 1297894-32-6): Yield: 88%; mp: 150°C; Purity (UPLC): t_R = 5.05 min, purity 99.6%. FT-IR υ_{max} (KBr, cm^{-1}): 2919 (CH aromatic), 1678 (C=O), 1598 (C=C aromatic), 1473 (C=N). ^{1}H-NMR (400 Hz, DMSO-d_6, ppm): δ = 8.10 (d, 2H, J = 6.8 *Hz* benzoyl H_{3+5}), 7.66 (d, 2H, J = 6.8 *Hz* benzoyl H_{2+6}), 7.53 (s, 2H, dimethylphenyl H_{2+6}), 7.24 (s, 1H, dimethylphenyl H_4), 5.15 (s, 2H, $-CH_2-$), 2.33 (s, 6H, $-CH_3$). Elemental Analysis Calcd. (%) for $C_{18}H_{15}ClN_2O_2S$ (358.84): C, 60.25; H, 4.21; N, 7.81; S, 8.94. Found: C, 60.21; H, 4.06; N, 7.86; S, 8.75.

5-(3,5-Dimethylphenyl)-2-[(4-bromobenzoyl)methyl]thio-1,3,4-oxadiazole (**3d**) (CAS Registry number: 1004367-76-3): Yield: 80%; mp: 162°C; Purity (UPLC): t_R = 5.24 min, purity 99.9%. FT-IR υ_{max} (KBr, cm^{-1}): 3090 (CH aromatic), 1680 (C=O), 1583 (C=C aromatic), 1473 (C=N). ^{1}H-NMR (400 Hz, DMSO-d_6, ppm): δ = 7.98 (d, 2H, J = 8 *Hz* benzoyl H_{3+5}), 7.80 (d, 2H, J = 8 *Hz* benzoyl H_{2+6}), 7.50 (s, 2H, dimethylphenyl H_{2+6}), 7.22 (s, 1H, dimethylphenyl H_4), 5.12 (s, 2H, $-CH_2-$) 2.31 (s, 6H, $-CH_3$). Elemental Analysis Calcd. (%) for $C_{18}H_{15}BrN_2O_2S$ (403.30): C, 53.61; H, 3.75; N, 6.95; S, 7.95. Found: C, 53.63; H, 3.76; N, 6.83; S, 7.70.

5-(3,5-Dimethylphenyl)-2-[(4-methylbenzoyl)methyl]thio-1,3,4-oxadiazole (**3e**) (CAS Registry number: 1330419-10-7): Yield: 83%; mp: 139°C; Purity (UPLC): t_R = 6.37 min, purity 99.4%. FT-IR υ_{max} (KBr, cm^{-1}): 2923 (CH aromatic), 1676 (C=O), 1604, 158 (C=C aromatic), 1473 (C=N). ^{1}H-NMR (400 Hz, DMSO-d_6, ppm): δ = 7.97 (d, 2H, J = 8.4 *Hz* benzoyl H_{3+5}), 7.50 (s, 2H, dimethylphenyl H_{2+6}), 7.38 (d, 2H, J = 8.4 *Hz* benzoyl H_{2+6}), 7.22 (s, 1H, dimethylphenyl H_4), 5.11 (s, 2H, $-CH_2-$), 2.38 (s, 3H, $-CH_3$), 2.31 (s, 6H, $-CH_3$). Elemental Analysis Calcd. (%) for $C_{19}H_{18}N_2O_2S$ (338.42): C, 67.43; H, 5.36; N, 8.28; S, 9.47. Found: C, 67.33; H, 5.28; N, 8.25; S, 9.39.

5-(3,5-Dimethylphenyl)-2-[(4-nitrobenzoyl)methyl]thio-1,3,4-oxadiazole (**3f**): Yield: 81%; mp: decomp.; Purity (UPLC): t_R = 5.12 min, purity 99.5%. FT-IR υ_{max} (KBr, cm^{-1}): 2916 (CH aromatic), 1685 (C=O), 1528 (C=C aromatic), 1474 (C=N). ^{1}H-NMR (400 Hz, DMSO-d_6, ppm): δ = 8.37 (d, 2H, J = 8.8 *Hz* benzoyl H_{3+5}), 8.28 (d, 2H, J = 8.8 *Hz* benzoyl H_{2+6}), 7.52 (s, 2H, dimethylphenyl H_{2+6}), 7.23 (s, 1H, dimethylphenyl H_4), 5.21 (s, 2H, $-CH_2-$), 2.06 (s, 6H, $-CH_3$). Elemental Analysis Calcd. (%) for $C_{18}H_{15}N_3O_4S$ (369.39): C, 58.53; H, 4.09; N, 11.38; S, 8.68. Found: C, 58.90; H, 4.11; N, 11.03; S, 8.37.

5-(3,4-Dimethylphenyl)-2-(benzoylmethyl)thio-1,3,4-oxadiazole (**4a**) (CAS Registry number: 850086-94-1): Yield: 81%; mp: 140°C; Purity (UPLC): t_R = 4.83 min, purity 100%. FT-IR υ_{max} (KBr, cm^{-1}): 2955 (CH aromatic), 1678 (C=O), 1595, 1579 (C=C aromatic), 1472 (C=N). ^{1}H-NMR (400 Hz, DMSO-d_6, ppm): δ = 8.07 (d, 2H, J = 7.2 *Hz* benzoyl H_{2+6}), 7.74 (t, 1H, J = 7.6 *Hz* benzoyl H_4), 7.79 (s, 1H, dimethylphenyl H_2), 7.66 (d, 1H, J = 6.4 *Hz*, dimethylphenyl H_6), 7.58 (d, 2H, J = 7.2 *Hz* benzoyl H_{3+5}), 7.34 (d, 1H, J = 6.4 *Hz*, dimethylphenyl H_5), 5.17 (s, 2H, $-CH_2-$), 2.29 (s, 3H, $-CH_3$), 2.28 (s, 3H, $-CH_3$). ^{13}C-NMR (400 Hz, DMSO-d_6, ppm): δ = 193.22 (C=O), 165.75 (oxadiazole C_5), 163.32 (oxadiazole C_2), 141.55, 138.11, 135.55, 134.51, 130.87, 129.40, 128.98, 127.52, 124.36, 120.94, 40.94 ($-CH_2-$), 19.98 ($-CH_3$), 19.69 ($-CH_3$). Elemental Analysis Calcd. (%) for $C_{18}H_{16}N_2O_2S$ (324.40): C, 66.64; H, 4.97; N, 8.64; S, 9.88. Found: C, 65.89; H, 5.06; N, 8.54; S, 9.73.

5-(3,4-Dimethylphenyl)-2-[(4-fluorobenzoyl)methyl]thio-1,3,4-oxadiazole (**4b**) (CAS Registry number: 849478-19-9): Yield: 69%; mp: 159°C; Purity (UPLC): t_R = 5.07 min, purity 99.9%. FT-IR υ_{max} (KBr, cm^{-1}): 3072 (CH aromatic), 1681 (C=O), 1590 (C=C aromatic), 1474 (C=N). ^{1}H-NMR (400 Hz, DMSO-d_6, ppm): δ = 8.17 (d, 2H, J = 7.6 *Hz* benzoyl H_{2+6}), 7.70 (s, 1H, dimetylphenyl H_2), 7.65 (d, 1H, J = 8 *Hz*, dimethylphenyl H_6), 7.43 (d, 2H, J = 7.6 *Hz* benzoyl H_{3+5}), 7.33 (d, 1H, J = 8 *Hz*, dimethylphenyl H_5), 5.16 (s, 2H, $-CH_2-$), 2.29 (s, 3H, $-CH_3$metil), 2.28 (s, 3H, $-CH_3$). Elemental Analysis Calcd. (%) for $C_{18}H_{15}FN_2O_2S$ (342.39): C, 63.14; H, 4.42; N, 8.18; S, 9.37. Found: C, 62.65; H, 4.28; N, 8.09; S, 9.22.

5-(3,4-Dimethylphenyl)-2-[(4-chlorobenzoyl)methyl]thio-1,3,4-oxadiazole (**4c**) (CAS Registry number: 1011852-13-3): Yield: 70%; mp: 149°C; Purity (UPLC): t_R = 6.46 min, purity 99.5%. FT-IR υ_{max} (KBr, cm^{-1}): 3088 (CH aromatic), 1677 (C=O), 1586 (C=C aromatic), 1475 (C=N). ^{1}H-NMR (400 Hz, DMSO-d_6, ppm): δ = 8.08 (d, 2H, J = 8 *Hz* benzoyl H_{2+6}), 7.69 (s, 1H, dimethylphenyl H_2), 7.67 (d, 1H, J = 8.4 *Hz*, dimethylphenyl H_6), 7.64 (d, 2H, J = 8 *Hz* benzoyl H_{3+5}), 7.33 (d, 1H, J = 8 *Hz*, dimethylphenyl H_5), 5.15 (s, 2H, $-CH_2-$), 2.29 (s, 3H, $-CH_3$), 2.28 (s, 3H, $-CH_3$). Elemental Analysis Calcd. (%) for $C_{18}H_{15}ClN_2O_2S$ (358.84): C, 60.25; H, 4.21; N, 7.81; S, 8.94. Found: C, 59.98; H, 4.17; N, 7.81; S, 8.87.

5-(3,4-Dimethylphenyl)-2-[(4-bromobenzoyl)methyl]thio-1,3,4-oxadiazole (**4d**) (CAS Registry number: 850030-38-5): Yield: 65%; mp: 165°C; Purity (UPLC): t_R = 7.01 min, purity 99.5%. FT-IR υ_{max} (KBr, cm^{-1}): 3088 (CH aromatic), 1678 (C=O), 1582 (C=C aromatic), 1475 (C=N). ^{1}H-NMR (400 Hz, DMSO-d_6, ppm): δ = 8.01 (d, 2H, J = 7.6 *Hz* benzoyl H_{2+6}), 7.81 (d, 2H, J = 7.6 *Hz* benzoyl H_{3+5}), 7.69

(s, 1H, dimethylphenyl H_2), 7.64 (d, 1H, J = 8.4 *Hz*, dimethylphenyl H_6), 7.33 (d, 1H, J = 8 *Hz*, dimethylphenyl H_5), 5.14 (s, 2H, $-CH_2-$), 2.29 (s, 3H, $-CH_3$), 2.28 (s, 3H, $-CH_3$). Elemental Analysis Calcd. (%) for $C_{18}H_{15}BrN_2O_2S$ (403.30): C, 53.61; H, 3.75; N, 6.95; S, 7.95. Found: C, 53.28; H, 3.70; N, 6.98; S, 7.94.

5-(3,4-Dimethylphenyl)-2-[(4-methylbenzoyl)methyl]thio-1,3,4-oxadiazole (**4e**) (CAS Registry number: 1011954-41-8): Yield: 72%; mp: 152°C; Purity (UPLC): t_R = 5.87 min, purity 99.8%. FT-IR υ_{max} (KBr, cm^{-1}): 3026 (CH aromatic), 1672 (C=O), 1603 (C=C aromatic), 1474 (C=N). ^{1}H-NMR (400 Hz, DMSO-d_6, ppm): δ = 7.98 (d, 2H, J = 8 *Hz* benzoyl H_{2+6}), 7.68 (s, 1H, dimethylphenyl H_2), 7.65 (d, 1H, J = 8 *Hz*, dimethylphenyl H_6), 7.39 (d, 2H, J = 8 *Hz* benzoyl H_{3+5}), 7.33 (d, 1H, J = 8 *Hz*, dimethylphenyl H_5), 5.13 (s, 2H, $-CH_2-$), 2.41 (s, 3H, $-CH_3$), 2.29 (s, 3H, $-CH_3$), 2.28 (s, 3H, $-CH_3$). Elemental Analysis Calcd. (%) for $C_{19}H_{18}N_2O_2S$ (338.42): C, 67.43; H, 5.36; N, 8.28; S, 9.47. Found: C, 67.64; H, 5.23; N, 8.32; S, 9.45.

5-(3,4-Dimethylphenyl)-2-[(4-nitrobenzoyl)methyl]thio-1,3,4-oxadiazole (**4f**) (CAS Registry number: 1011901-88-4): Yield: 60%; mp: decomp.; Purity (UPLC): t_R = 4.73 min, purity 100%. FT-IR υ_{max} (KBr, cm^{-1}): 3065 (CH aromatic), 1684 (C=O), 1527 (C=C aromatic), 1477 (C=N). ^{1}H-NMR (400 Hz, DMSO-d_6, ppm): δ = 8.40 (d, 2H, J = 9.2 *Hz* benzoyl H_{2+6}), 8.29 (d, 2H, J = 9.2 *Hz* benzoyl H_{3+5}), 7.70 (s, 1H, dimethylphenyl H_2), 7.65 (d, 1H, J = 7.6 *Hz*, dimethylphenyl H_6), 7.33 (d, 1H, J = 8 *Hz*, dimethylphenyl H_5), 5.22 (s, 2H, $-CH_2-$), 2.29 (s, 3H, $-CH_3$), 2.28 (s, 3H, $-CH_3$). Elemental Analysis Calcd. (%) for $C_{18}H_{15}N_3O_4S$ (369.39): C, 58.53; H, 4.09; N, 11.38; S, 8.68. Found: C, 58.18; H, 4.00; N, 11.37; S, 8.66.

4.1.5 | General procedure for the synthesis of **5a–e** and **6a–e**

To the solution of appropriate ketone derivative **3a–f**, **4a–f** in acetic acid (15 mL), hydrazine hydrate (0.02 mol) was added. The mixture was stirred and refluxed for 4 h. The formed precipitate was filtered and washed with ethanol. The residue was crystallized from acetonitrile.[22]

6-(3,5-Dimethylphenyl)-3-(phenyl)-7*H*-1,2,4-triazolo[3,4-*b*][1,3,4]thiadiazine (**5a**): Yield: 71%; mp: 219°C; Purity (UPLC): t_R = 3.03 min, purity 98.8%. FT-IR υ_{max} (KBr, cm^{-1}): 2925 (CH aromatic), 1592 (C=C aromatic), 1457 (C=N). ^{1}H-NMR (400 Hz, DMSO-d_6, ppm): δ = 8.00 (d, 2H, J = 6.4 Hz, phenyl H_{2+6}), 7.63–7.56 (m, 5H, phenyl H_{3+4+5} + dimethylphenyl H_{2+6}), 7.19 (s, 1H, dimethylphenyl H_4), 4.44 (s, 2H, $-CH_2-$), 2.36 (s, 6H, $-CH_3$). ^{13}C-NMR (400 Hz, pyridine, ppm): δ = 156.00 (N=C–S), 154.40 (N=C), 143.84 (N=C–N), 139.63, 135.70, 130.73, 133.39, 133.32, 129.17, 128.33, 127. 80, 24.92 ($-S-CH_2-$), 22.42 ($-CH_3$). Elemental Analysis Calcd. (%) for $C_{18}H_{16}N_4S$ (320.41): C, 67.47; H, 5.03; N, 17.49; S, 10.01. Found: C, 67.60; H, 4.95; N, 17.38; S, 9.88.

6-(3,5-Dimethylphenyl)-3-(4-fluorophenyl)-7*H*-1,2,4-triazolo[3,4-*b*][1,3,4]thiadiazine (**5b**): Yield: 65%; mp: 265°C; Purity (UPLC): t_R = 3.09 min, purity 98.6%. FT-IR υ_{max} (KBr, cm^{-1}): 2992 (CH aromatic), 1602 (C=C aromatic), 1463 (C=N). ^{1}H-NMR (400 Hz, DMSO-d_6, ppm): δ = 8.08 (d, 2H, J = 5.6 Hz, phenyl H_{3+5}), 7.62 (s, 2H, dimethylphenyl H_{2+6}), 7.44 (d, 2H, J = 5.6 Hz, phenyl H_{2+6}), 7.19 (s, 1H, dimethylphenyl H_4), 4.43 (s, 2H, $-CH_2-$), 2.36 (s, 6H, $-CH_3$). Elemental Analysis Calcd. (%) for $C_{18}H_{15}FN_4S$ (338.40): C, 63.89; H, 4.47; N, 16.56; S, 9.48. Found: C, 63.72; H, 4.38; N, 16.50; S, 9.43.

6-(3,5-Dimethylphenyl)-3-(4-chlorophenyl)-7*H*-1,2,4-triazolo[3,4-*b*][1,3,4]thiadiazine (**5c**): Yield: 60%; mp: 263°C; Purity (UPLC): t_R = 3.88 min, purity 98.7%. FT-IR υ_{max} (KBr, cm^{-1}): 2917 (CH aromatic), 1520 (C=C aromatic), 1461 (C=N). ^{1}H-NMR (400 Hz, DMSO-d_6, ppm): δ = 8.08 (d, 2H, J = 8.4 Hz, phenyl H_{3+5}), 7.67 (d, 2H, J = 8.4 Hz, phenyl $_{H2+6}$), 7.60 (s, 2H, dimethylphenyl H_{2+6}), 7.19 (s, 1H, dimethylphenyl H_4), 4.42 (s, 2H, $-CH_2-$), 2.36 (s, 6H, $-CH_3$). Elemental Analysis Calcd. (%) for $C_{18}H_{15}ClN_4S$ (354.86): C, 60.92; H, 4.26; N, 15.79; S, 9.04. Found: C, 60.73; H, 4.16; N, 15.76; S, 9.04.

6-(3,5-Dimethylphenyl)-3-(4-bromophenyl)-7*H*-1,2,4-triazolo[3,4-*b*][1,3,4]thiadiazine (**5d**): Yield: 80%; mp: decomp.; Purity (UPLC): t_R = 3.63 min, purity 98.0%. FT-IR υ_{max} (KBr, cm^{-1}): 2994 (CH aromatic), 1586 (C=C aromatic), 1466 (C=N). ^{1}H-NMR (400 Hz, DMSO-d_6, ppm): δ = 7.94 (d, 2H, J = 8 Hz, phenyl H_{3+5}), 7.81 (d, 2H, J = 8 Hz, phenyl H_{2+6}), 7.61 (s, 2H, dimethylphenyl H_{2+6}), 7.19 (s, 1H, dimethylphenyl H_4), 4.42 (s, 2H, $-CH_2-$), 2.36 (s, 6H, $-CH_3$). Elemental Analysis Calcd. (%) for $C_{18}H_{15}BrN_4S$ (399.31): C, 54.14; H, 3.79; N, 14.03; S, 8.03. Found: C, 53.70; H, 3.76; N, 13.94; S, 8.01.

6-(3,5-Dimethylphenyl)-3-(4-methylphenyl)-7*H*-1,2,4-triazolo[3,4-*b*][1,3,4]thiadiazine (**5e**): Yield: 75%; mp: 233°C; Purity (UPLC): t_R = 3.62 min, purity 97.9%. FT-IR υ_{max} (KBr, cm^{-1}): 2998 (CH aromatic), 1608 (C=C aromatic), 1463 (C=N). ^{1}H-NMR (400 Hz, DMSO-d_6, ppm): δ = 7.91 (d, 2H, J = 8 Hz, phenyl H_{3+5}), 7.64 (s, 2H, dimethylphenyl H_{2+6}), 7.4 (d, 2H, J = 8 Hz, phenyl H_{2+6}), 7.19 (s, 1H, dimethylphenyl H_4), 4.41 (s, 2H, $-CH_2-$), 2.40 (s, 3H, $-CH_3$), 2.36 (s, 6H, $-CH_3$). Elemental Analysis Calcd. (%) for $C_{19}H_{18}N_4S$ (334.44): C, 68.23; H, 5.42; N, 16.75; S, 9.59. Found: C, 68.08; H, 5.50; N, 16.37; S, 9.53.

6-(3,4-Dimethylphenyl)-3-(phenyl)-7*H*-1,2,4-triazolo[3,4-*b*][1,3,4]thiadiazine (**6a**): Yield: 71%; mp: 219°C; Purity (UPLC): t_R = 3.68 min, purity 99.3%. FT-IR υ_{max} (KBr, cm^{-1}): 2925 (CH aromatic), 1592 (C=C aromatic), 1457 (C=N). ^{1}H-NMR (400 Hz, DMSO-d_6, ppm): δ = 8.01 (d, 2H, J = 6.4 Hz, phenyl H_{2+6}), 7.81 (s, 1H, dimethylphenyl H_2), 7.73 (d, 1H, J = 7.6 Hz, dimethylphenyl H_6), 7.64–7.56 (m, 3H, phenyl H_{3+4+5}), 7.33 (d, 1H, J = 7.6 Hz, dimethylphenyl H_5), 4.44 (s, 2H, $-CH_2-$), 2.32 (s, 3H, $-CH_3$), 2.31 (s, 3H, $-CH_3$). ^{13}C-NMR (400 Hz, pyridine, ppm): δ = 156.13 (N=C–S), 154.30 (N=C), 143.61 (N=C–N), 140.40, 138.40, 135.67, 133.30, 131.45, 130.98, 130.67, 129.14,127.45, 126.04, 24.90 ($-S-CH_2-$), 20.92 ($-CH_3$), 20.86 ($-CH_3$). Elemental Analysis Calcd. (%) for $C_{18}H_{16}N_4S$ (320.41): C, 67.47; H, 5.03; N, 17.49; S, 10.01. Found: C, 66.97; H, 5.03; N, 17.33; S, 9.90.

6-(3,4-Dimethylphenyl)-3-(4-fluorophenyl)-7*H*-1,2,4-triazolo[3,4-*b*][1,3,4]thiadiazine (**6b**): Yield: 50%; mp: 245°C; Purity (UPLC): t_R = 2.95 min, purity 99.0%. FT-IR υ_{max} (KBr, cm^{-1}): 2907 (CH aromatic), 1600 (C=C aromatic), 1458 (C=N). ^{1}H-NMR (400 Hz, DMSO-d_6, ppm): δ = 8.07 (d, 2H, J = 8.8 Hz, phenyl H_{3+5}), 7.80 (s, 1H, dimethylphenyl H_2), 7.71 (d, 1H, J = 7.6 Hz, dimethylphenyl H_6), 7.43 (d, 2H, J = 8.8 Hz, phenyl H_{2+6}), 7.33 (d, 1H, J = 7.6 Hz,

dimethylphenyl H_5), 4.43 (s, 2H, $-CH_2-$), 2.32 (s, 3H, $-CH_3$), 2.31 (s, 3H, $-CH_3$). Elemental Analysis Calcd. (%) for $C_{18}H_{15}FN_4S$ (338.40): C, 63.89; H, 4.47; N, 16.56; S, 9.48. Found: C, 63.71; H, 4.91; N, 16.71; S, 9.02.

6-(3,4-Dimethylphenyl)-3-(4-chlorophenyl)-7*H*-1,2,4-triazolo[3,4-*b*][1,3,4]thiadiazine (**6c**): Yield: 64%; mp: 236°C; Purity (UPLC): t_R = 3.67 min, purity 98.7%. FT-IR υ_{max} (KBr, cm^{-1}): 3035 (CH aromatic), 1589 (C=C aromatic), 1462 (C=N). ^{1}H-NMR (400 Hz, DMSO-d_6, ppm): δ = 8.02 (d, 2H, J = 9.2 Hz, phenyl H_{3+5}), 7.90 (s, 1H, dimethylphenyl H_2), 7.70 (d, 1H, J = 8 Hz, dimethylphenyl H_6), 7.67 (d, 2H, J = 9.2 Hz, phenyl H_{2+6}), 7.33 (d, 1H, J = 8 Hz, dimethylphenyl H_5), 4.42 (s, 2H, $-CH_2-$), 2.32 (s, 3H, $-CH_3$), 2.31 (s, 3H, $-CH_3$). ^{13}C-NMR (400 Hz, pyridine, ppm): δ = 153.61 (N=C–S), 152.79 (N=C), 142.03 (N=C–N), 139.04, 137.66, 136.94, 132.75, 129.97, 129.53, 129.35, 129.18, 125.97, 124.46, 23.16 ($-S-CH_2-$), 19.40 ($-CH_3$). Elemental Analysis Calcd. (%) for $C_{18}H_{15}ClN_4S$ (354.86): C, 60.92; H, 4.26; N, 15.79; S, 9.04. Found: C, 60.80; H, 4.26; N, 15.71; S, 9.00.

6-(3,4-Dimethylphenyl)-3-(4-bromophenyl)-7*H*-1,2,4-triazolo[3,4-*b*][1,3,4]thiadiazine (**6d**): Yield: 60%; mp: 242°C; Purity (UPLC): t_R = 4.08 min, purity 99.7%. FT-IR υ_{max} (KBr, cm^{-1}): 2984 (CH aromatic), 1586 (C=C aromatic), 1462 (C=N). ^{1}H-NMR (400 Hz, DMSO-d_6, ppm): δ = 7.94 (d, 2H, J = 8 Hz, phenyl H_{3+5}), 7.81 (d, 2H J = 8 Hz, phenyl H_{2+6}), 7.79 (s, 1H, dimethyl H_2), 7.70 (d, 1H, J = 7.6 Hz, dimethylphenyl H_6), 7.33 (d, 1H, J = 7.6 Hz, dimethylphenyl H_5), 4.42 (s, 2H, $-CH_2-$), 2.32 (s, 3H, $-CH_3$), 2.31 (s, 3H, $-CH_3$). ^{13}C-NMR (400 Hz, pyridine, ppm): δ = 153.71 (N=C–S), 152.84 (N=C), 142.02 (N=C–N), 139.03, 136.95, 133.18, 132.35, 129.98, 129.56, 129.51, 129.30, 126.41, 125.98, 124.48, 23.20 ($-S-CH_2-$), 19.43 ($-CH_3$), 19.36 ($-CH_3$). Elemental Analysis Calcd. (%) for $C_{18}H_{15}BrN_4S$ (399.31): C, 54.14; H, 3.79; N, 14.03; S, 8.03. Found: C, 53.73; H, 3.80; N, 13.69; S, 7.90.

6-(3,4-Dimethylphenyl)-3-(4-methylphenyl)-7*H*-1,2,4-triazolo[3,4-*b*][1,3,4]thiadiazine (**6e**): Yield: 40%; mp: 206°C; Purity (UPLC): t_R = 3.61 min, purity 98.6%. FT-IR υ_{max} (KBr, cm^{-1}): 2970 (CH aromatic), 1611 (C=C aromatic), 1459 (C=N). ^{1}H-NMR (400 Hz, DMSO-d_6, ppm): δ = 7.92 (d, 2H, J = 8.4 Hz, phenyl H_{3+5}), 7.82 (s, 1H, dimethylphenyl H_2), 7.73 (d, 1H, J = 8 Hz, dimethylphenyl H_6), 7.39 (d, 2H J = 8.4 Hz, phenyl H_{2+6}), 7.33 (d, 1H, J = 8 Hz, dimethylphenyl H_5), 4.41 (s, 2H, $-CH_2-$), 2.31 (s, 3H, $-CH_3$), 2.32 (s, 3H, $-CH_3$), 2.31 (s, 3H, $-CH_3$). ^{13}C-NMR (400 Hz, pyridine, ppm): δ = 156.13 (N=C–S), 154.24 (N=C), 149.90 (N=C–N), 143.70, 140.44, 138.35, 132.86, 131.45, 131.39, 131.03, 129.13, 127.57, 126.12, 24.46 ($-S-CH_2-$), 22.13 ($-CH_3$), 20.55 ($-CH_3$). Elemental Analysis Calcd. (%) for $C_{19}H_{18}N_4S$ (334.44): C, 68.23; H, 5.42; N, 16.75; S, 9.59. Found: C, 68.05; H, 5.46; N, 16.67; S, 9.53.

4.2 | Pharmacological/biological assays

4.2.1 | Cell viability

The murine macrophage RAW264.7 cell line (American Type Culture Collection) was maintained in Dulbecco's modified Eagle's medium High Glucose supplemented with 10% fetal bovine serum and 1% penicillin (10.000 units/mL) and streptomycin (10.000 µg/mL) at 37°C under a 5% CO_2 atmosphere. Cell viability was measured by using 3-(4,5-dimethylthiazol-2-yl)-2,5-diphenyltetrazolium bromide (MTT) colorimetric assay, which depends on the mitochondria-based reduction of MTT formazan. Plated RAW264.7 cells were treated with various concentrations of compounds (50–100 µM). After 24 h, the cell medium was discarded and MTT solution (0.5 mg/mL) was added to wells for an additional 2 h at 37°C. After incubation, the cell culture medium was removed and 100 µL of isopropanol was used to dissolve formazan. The absorbance was determined at 570 nm wavelength by a microplate reader (Thermo Multiscan Spectrum). The absorbance of the control group was considered as 100%. The percentage of cell viability was calculated as follows:[23,24]

$$\%\text{Viability} = \frac{(\text{Absorbance of treatment group})}{(\text{Absorbance of control})} \times 100.$$

4.2.2 | NO inhibition assay

The anti-inflammatory activity of compounds was evaluated by measuring the stable NO metabolite, nitrite, levels in cell culture media, with Griess reagent. RAW264.7 cells were plated, with a density of 1×10^6 cells/mL, into a 48-well plate and incubated for 24 h at 37°C in 5% CO_2. After the cell culture medium was aspirated, cells were pretreated with various concentrations of compounds (50–100 µM) for 2 h and then stimulated with 1 µg/mL of LPS (LPS from *Escherichia coli* 0111:B4; Sigma-Aldrich) for an additional 22 h. The collected culture supernatant was mixed with an equal volume of Griess reagent (1% sulfanilamide and 0.1% *N*-(1-naphthyl)ethylenediamine dihydrochloride in 5% phosphoric acid) in a 96-well plate and incubated at room temperature for 10 min in the dark. The absorbance was determined using a microplate reader (Multiscan Ascent) at 540 nm wavelength. The concentration of nitrite in samples was calculated by using the sodium nitrite standard curve. Indomethacin (100 µM) was used as a positive control.[23,24]

4.2.3 | PGE_2 inhibition assay

PGE_2 concentrations in cell culture supernatants of the compounds that have shown to reduce inflammation in NO assay were measured by using a commercially available quantitative ELISA kit (Abcam PGE_2 ELISA Kit) according to the manufacturer's instructions.[23]

4.2.4 | IL-6 releasing inhibition assay

RAW264.7 cells were pretreated with the isolates for 2 h and then stimulated with LPS (1 µg/mL) for 22 h. Samples were diluted five times due to their high IL-6 value. The concentration of IL-6 was assayed using the commercially available quantitative ELISA kit (Invitrogen) according to the manufacturer's instructions.[25]

4.2.5 | iNOS inhibition assay

iNOS catalyzes the production of NO from L-arginine, which is used in various cell signaling events. iNOS, an inducible member of the NOS family, is upregulated as a host-defense mechanism during proinflammatory cytokine activity. The iNOS enzyme activity of the compounds in the cell lysate will be measured using a commercially available quantitative ELISA kit (Abcam iNOS ELISA Kit) according to the manufacturer's instructions.[26]

4.2.6 | Statistical analysis

All experiments were conducted in triplicate. The statistical analyses were conducted using the GraphPad Prism 8 (GraphPad Software, Inc.; version 8.4.3). Differences between groups were determined by using one-way analysis of variance (ANOVA) following the post-hoc tests by Tukey.

4.3 | Molecular docking

Docking studies were performed using Schrödinger's GLIDE (version 2019.01)[27,28] the crystal structure of the iNOS enzyme (PDB ID: 3E7G). The crystal structure was downloaded from the PDB[29] and prepared with Schrödinger's Protein Preparation Wizard tool using default settings.[30] Before protein preparation, water molecules were removed by leaving protoporphyrin IX at the binding site. Protonation states were assigned using Schrödinger's PROPKA with pH 7.0, and hydrogen bond geometries were then optimized. Finally, the energy minimization step was carried out using the OPLS3 force and default settings. Then, the Receptor Grid Generation[31] was applied by selecting the coordinates of the co-crystallized inhibitor. To test whether the docking program could accurately reproduce the binding mode of the co-crystallized inhibitor, redocking experiments were performed before docking studies of our compounds. Glide Score (SP) and "sample ring conformation" mode were used to generate the docking poses. The suitable pose was evaluated based on the root mean square deviation (RMSD) of the co-crystallized conformation with the predicted conformation based on the principle that the docking pose with RMSD less than 2.0 Å is compatible with the X-ray structure. The predicted docking poses for iNOS reproduced the co-crystallized binding modes and interactions with an RMSD value of 0.595 Å. Therefore, this docking program and settings were also used in studies of our own compounds. The data set of derivatives was created by generating possible ionization states (pH 7.0 ± 1.0) with Schrödinger's LigPrep[32] tool. Then, 64 conformers were generated for each molecule using ConfGen.[33,34] Conformers were also generated for co-crystallized inhibitors before redocking studies using the indicated settings.

ACKNOWLEDGMENTS

The authors thank Assoc. Prof. Ebru Turkoz Acar and Pharm. Ecesu Sezen to support developing the method of UPLC analysis. This work was supported by Yeditepe University within the scope of Yeditepe University Research Projects and Scientific Activities of Yeditepe University (YAP). Project number: YAP-AP-SAB-22025.

CONFLICTS OF INTEREST STATEMENT

The authors declare no conflicts of interest.

DATA AVAILABILITY STATEMENT

Research data are not shared.

ORCID

Wolfgang Sippl http://orcid.org/0000-0002-5985-9261
Meric Koksal http://orcid.org/0000-0001-7662-9364

REFERENCES

[1] T. L. Lemke, D. A. Williams, V. F. Roche, S. W. Zito, *Foye's Principles of Medicinal Chemistry*, Wolters Kluwer/Lippincott Williams&Wilkins, Tokyo **2013**.
[2] O. Takeuchi, S. Akira, *Cell* **2010**, *140*, 805. https://doi.org/10.1016/j.cell.2010.01.022
[3] L. Chen, H. Deng, H. Cui, J. Fang, Z. Zuo, J. Deng, Y. Li, X. Wang, L. Zhao, *Oncotarget* **2018**, *9*, 7204. https://doi.org/10.18632/oncotarget.23208
[4] M. M. Al-Sanea, M. S. Abdel-Maksoud, M. F. El-Behairy, A. Hamdi, H. U. Rahman, D. G. T. Parambi, R. M. Elbargisy, A. A. B. Mohamed, *Bioorg. Chem.* **2023**, *139*, 106716. https://doi.org/10.1016/J.BIOORG.2023.106716
[5] D. M. da Silva, H. Langer, T. Graf, *Int. J. Mol. Sci.* **2019**, *20*, 2322. https://doi.org/10.3390/ijms20092322
[6] S. Gordon, P. R. Taylor, *Nat. Rev. Immunol.* **2005**, *5*, 953.
[7] A. Cardeno, M. Aparicio-Soto, S. Montserrat-de la Paz, B. Bermudez, F. J. G. Muriana, C. Alarcon-de-la-Lastra, *J. Func. Foods.* **2015**, *14*, 779. https://doi.org/10.1016/j.jff.2015.03.009
[8] G. Singh, G. Singh, R. Bhatti, M. Gupta, A. Kumar, A. Sharma, M. P. Singh Ishar, *Eur. J. Med. Chem.* **2018**, *153*, 56. https://doi.org/10.1016/j.ejmech.2018.04.004
[9] J. J. Watters, J. A. Sommer, Z. A. Pfeiffer, U. Prabhu, A. N. Guerra, P. J. Bertics, *J. Biol. Chem.* **2002**, *277*(11), 9077. https://doi.org/10.1016/S0021-9258(18)42133-3
[10] M. M. G. El-Din, M. I. El-Gamal, M. S. Abdel-Maksoud, H. Lee, J. Choi, T. Kim, J. Shin, H. Lee, H. Kim, K. Lee, D. Baek, *Bioorg. Med. Chem. Lett.* **2020**, *30*, 126884. https://doi.org/10.1016/j.bmcl.2019.126884
[11] M. F. A. Mohamed, A. A. Marzouk, A. ç Nafady, D. A. El-Gamal, R. M. Allam, G. E. A. Abuo-Rahma, H. I. E. Subbagh, A. mH. Moustafa, *Bioorg. Chem.* **2020**, *105*, 104439. https://doi.org/10.1016/j.bioorg.2020.104439
[12] T. Ozyazici, E. E. Gurdal, D. Orak, H. Sipahi, T. Ercetin, H. O. Gulcan, M. Koksal, *Arch. Pharm.* **2020**, *353*, e2000061. https://doi.org/10.1002/ardp.202000061
[13] S. Li, J. Chou, S. Tsai, C. Tseng, C. Chung, W. Zeng, Y. Hu, N. Uramaru, G. Huang, F. Wong, *Eur. J. Med. Chem.* **2023**, *257*, 115496. https://doi.org/10.1016/j.ejmech.2023.115496
[14] H. L. Jang, M. I. El-Gamal, H. E. Choi, H. Y. Choi, K. T. Lee, C. H. oh, *Bioorg. Med. Chem. Lett.* **2014**, *24*, 571. https://doi.org/10.1016/j.bmcl.2013.12.018
[15] S. M. M. Faudzi, M. A. Abdullah, M. R. A. Manap, A. Z. Ismail, K. Rullah, M. F. F. M. Aluwi, A. N. M. Ramli, F. Abas, N. H. Lajis, *Bioorg. Chem.* **2020**, *94*, 103376. https://doi.org/10.1016/j.bioorg.2019.103376
[16] M. Akhtar, J. Niu, Y. Zhu, Z. Luo, T. Tian, Y. Dong, Y. Wang, M. S. Fareed, L. Lin, *Eur. J. Med. Chem.* **2023**, *256*, 115412. https://doi.org/10.1016/j.ejmech.2008.09.005

[17] S. V. Bhandari, K. G. Bothara, M. K. Raut, A. A. Patil, A. P. Sarkate, V. J. Mokale, *Bioorg. Med. Chem.* **2008**, *16*, 1822. https://doi.org/10.1016/j.bmc.2007.11.014
[18] H. Khalilullah, M. J. Ahsan, M. Hedaitullah, S. Khan, B. Ahmed, *Mini-Rev. Med. Chem.* **2012**, *12*, 789. https://doi.org/10.2174/138955712801264800
[19] M. Koksal, S. S. Bilge, A. Bozkurt, Z. S. Sahin, S. Isik, D. D. Erol, *Arzneimittel-Forschung* **2008**, *58*, 510. https://doi.org/10.1055/s-0031-1296550
[20] S. M. Edward, Merck Co., *USA PCT Int. Appl.* WO 2004, 45, 508 (Cl. A61k), 3 Jun 2004, US Appl. PV426, 529, 40 pp; CA **2002**, *141*, 23432m.
[21] G. Karabanovich, J. Zemanová, T. Smutný, R. Székely, M. Šarkan, I. Centárová, A. Vocat, I. Pávková, P. Čonka, J. Němeček, J. Stolaříková, M. Vejsová, K. Vávrová, V. Klimešová, A. Hrabálek, P. Pávek, S. T. Cole, K. Mikušová, J. Roh, *J. Med. Chem.* **2016**, *59*, 2362. https://doi.org/10.1021/acs.jmedchem.5b00608
[22] M. Koksal, I. Ozkan, M. Yarim, S. S. Bilge, A. Bozkurt, D. D. Erol, *Rev. Chim.* **2011**, *62*, 1069.
[23] M. E. Okur, A. E. Karadağ, Y. Özhan, H. Sipahi, Ş. Ayla, B. Daylan, Ş. Kültür,. Demirci, F. Demirci, *J. Ethnopharmacol.* **2021**, *266*, 113408. https://doi.org/10.1016/j.jep.2020.113408
[24] M. E. Okur, A. E. Karadağ, N. Üstündağ Okur, Y. Özhan, H. Sipahi, Ş. Ayla, B. Daylan, B. Demirci, F. Demirci, *Molecules* **2020**, *25*, 2695. https://doi.org/10.3390/molecules25112695
[25] M. Erdoğan, R. Konya, Y. Özhan, H. Sipahi, İ. Çinbilgel, M. Masullo, S. Piacente, H. Kırmızıbekmez, *S. Afr. J. Bot.* **2021**, *139*, 12. https://doi.org/10.1016/j.sajb.2021.01.028
[26] R. Minhas, Y. Bansal, G. Bansal, *Med. Res. Rev.* **2020**, *40*, 823. https://doi.org/10.1002/med.21636
[27] R. A. Friesner, R. B. Murphy, M. P. Repasky, L. L. Frye, J. R. Greenwood, T. A. Halgren, P. C. Sanschagrin, D. T. Mainz, *J. Med. Chem.* **2006**, *49*, 6177. https://doi.org/10.1021/jm051256o
[28] Schrödinger Release 2019-4: *Glide*, Schrödinger, LLC. New York, NY **2019**.
[29] H. M. Berman, T. Battistuz, T. N. Bhat, W. F. Bluhm, P. E. Bourne, K. Burkhardt, Z. Feng, G. L. Gilliland, L. Iype, S. Jain, P. Fagan, J. Marvin, D. Padilla, V. Ravichandran, B. Schneider, N. Thanki, H. Weissig, J. D. Westbrook, C. Zardecki, *Acta Crystallogr. D. Biol. Crystallogr.* **2002**, *58*, 899.
[30] Schrödinger Release 2019-4: *Protein Preparation Wizard; Epik*, Schrödinger, LLC, New York, NY, 2019; *Impact*, Schrödinger, LLC, New York, NY; *Prime*, Schrödinger, LLC, NewYork, NY, 2019.
[31] Schrödinger Release 2019-4: *Maestro*, Schrödinger, LLC, New York, NY, 2019.
[32] Schrödinger Release 2019-4: *LigPrep*, Schrödinger, LLC, New York, NY, 2019.
[33] Schrödinger Release 2019-4: *ConfGen*, Schrödinger, LLC, New York, NY, 2019.
[34] K. S. Watts, P. Dalal, R. B. Murphy, W. Sherman, R. A. Friesner, J. C. Shelley, *J. Chem. Inf. Model.* **2010**, *50*, 534. https://doi.org/10.1021/ci100015j

SUPPORTING INFORMATION

Additional supporting information can be found online in the Supporting Information section at the end of this article.

How to cite this article: A. Erdogan, Y. Ozhan, H. Sipahi, E. E. Gurdal, W. Sippl, M. Koksal, *Arch. Pharm.* **2024**;*357*:e2400238. https://doi.org/10.1002/ardp.202400238